# Journal of Materials Chemistry C

Accepted Manuscript


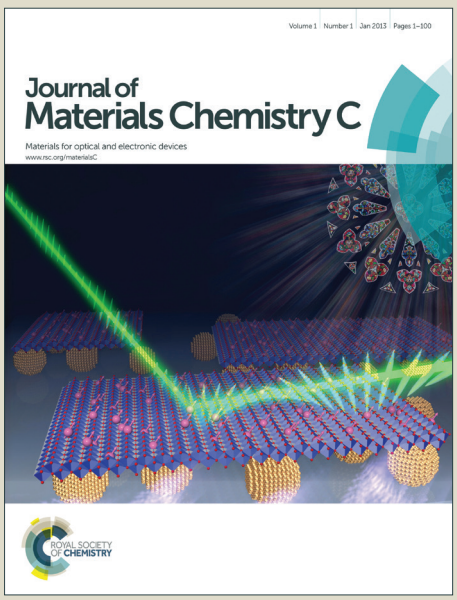





ROYAL SOCIETY OF CHEMISTRY

www.rsc.org/materialsC

Cite this: DOI: 10.1039/c0xx00000x

www.rsc.org/xxxxxx

PAPER

# Ultrahigh ferroelectric response in Fe modified $0.95(Na_{1/2}Bi_{1/2})TiO_3$-$0.05BaTiO_3$ single crystals

**Haiwu Zhang[a, b]*, Chao Chen[a, b], Hao Deng[a, b], Bo Ren[a], Xiangyong Zhao[a], Di Lin[a], Xiaobing Li[a], and Haosu Luo[a]***

Single crystals of x at.% Fe+$0.95(Na_{1/2}Bi_{1/2})TiO_3$-$0.05BaTiO_3$ (x%-Fe:NBBT5, x=0.1, 0.2 and 0.5) with ultrahigh ferroelectric response were developed by introducing $(Fe'_{Ti}-V_O^{\bullet\bullet})^{\bullet}$ defect associations. The giant field-induced bipolar and unipolar strains, i.e. $S_{max}$~1.1%, $\varepsilon_{max}/E_{max}$ ~1300 pm/V, $d_{33}$~600 pC/N and permittivity tunability ~120% demonstrate that they are promising candidates as lead-free ferroelectrics. The presence of ferromagnetic properties further provides new application potential as multiferroic materials. The defect chemistry and domain structure were studied systematically. The effects of microscopic defect functional centers on macroscopic properties were discussed in detail.

## 1. Introduction

Relaxor ferroelectrics are widely used in electromechanical devices such as sensors, transducers and actuators. However, the rising environmental protection awareness in nowadays are driving the search for environmental-friendly piezoelectric materials that can substitute the toxic lead-based counterparts. $Na_{1/2}Bi_{1/2}TiO_3$-based materials have attracted increasing interest due to their strong ferroelectric polarization and desirable characterizes such as tunable complexity in the phases, high-fatigue resistance, large field induced strain, etc.[1-4] Nevertheless, ferroelectric properties of NBT-based ferroelectrics are still inferior to those Pb-based ones and the relative high leakage current density and dielectric loss are still limiting their wide application in practical.[5] Therefore, clarifying the structure nature and further improving their ferroelectric performance have been the subject of ongoing investigations.

The ferroelectric properties are typically tailored by donor- or acceptor-doping, giving rise to ferroelectrically "soft effect" and "hard effect".[6, 7] In particular, the striking "hardening" effect of iron doping on decreasing the permittivity and piezoelectric constant as well as increasing the resistivity in $Pb(Zr_xTi_{1-x})O_3$ (PZT) ceramics attracts special interest.[8, 9] Besides, the ferromagnetic characteristics of iron functional centers provides new possibility for developing single-phase multiferroics. The underlying mechanisms, however, are still not clear up to now. According to the "volume effect", the defect dipoles aligning along the spontaneous polarization is energetically favorable, which will generate a restoring force for domain switching during aging.[10] The "boundary effect" (or "domain wall effect") suggests that the defects tend to migrate to domain walls to neutralize internals stresses and charges and consequently pin the domain walls.[11] However, recent studies by P. Jakes *et al.* proposed that the defect complexes are located within domains and rather than domain walls in unpoled samples based on their electric paramagnetic resonance spectrum (EPR) results.[12] Compared to ceramics, single crystals have homogeneous compositions and thus are more suitable for revealing the intrinsic mechanisms. Therefore, study on the microscopic defect structure and their effects on macroscopic physical properties of iron doped NBT-based single crystals is interesting not only for scientific reasons, but also from the point view of application.

In this work, x at.% Fe+$0.95(Na_{1/2}Bi_{1/2})TiO_3$-$0.05BaTiO_3$ (x%-Fe:NBBT5, x=0.1, 0.2 and 0.5) single crystals were grown using a top-seeded solution growth method (TSSG). The dielectric, piezoelectric and ferroelectric properties of the as-grown single crystals were studied systematically. The site occupation and valence state of iron were characterized using EPR measurements. Temperature dependent complex impedance spectra were measured and activation energy of corresponding defects was calculated accordingly. The ferroelectric domain structure was also studied, with particular emphasis on the interaction mechanism of chemical defects with domain structures.

## 2. Experimental

Single crystals of x%-Fe:NBBT5 (x=0.1, 0.2 and 0.5) were grown using the TSSG technique. This BT composition is close to the morphotropic phase boundary (MPB) and exhibits

excellent piezoelectric properties.[13] The as-grown single crystals were cut along the pseudocubic (0 0 1)/(1 0 0)/(0 1 0) planes with dimensions of 5×5×0.5 mm$^3$. All the samples were electroded by sputtering with gold on the two main faces. The polarization (*P-E*) and strain (*S-E*) hysteresis loops were measured using a ferroelectric test system (aixACCT TF-analyzer 1000). The electric-field dependent dielectric permittivity was tested using a Keithley 2410 (Cleveland, OH) high-voltage and a TH2816ALCR (Changzhou, China) analyzer. The frequency dependent dielectric properties were measured using a Novelcontrol CmbH Concept 40 broadband dielectric spectrometer. The piezoelectric constant ($d_{33}$) was measured by a quasi-static $d_{33}$ meter of Berlincourt type at about 55Hz. X-band (9.8GHz) EPR spectra were measured on a Bruker EMX spectrometer (Karlsruhe, Germany) at ambient temperature. The room temperature *M-H* curves were measured using the Vibrating Sample Magnetometer (Lake Share 7400, Lake Share Corporation, USA), which were calibrated using Ni standard sample. The temperature dependent complex impedance spectrum was measured using the Agilent 4294 impedance analyzer. Domain structures were observed by using a Olympus U-CMAD3 polarizing microscope set with a 0°/90° crossed polarizer analyzer.

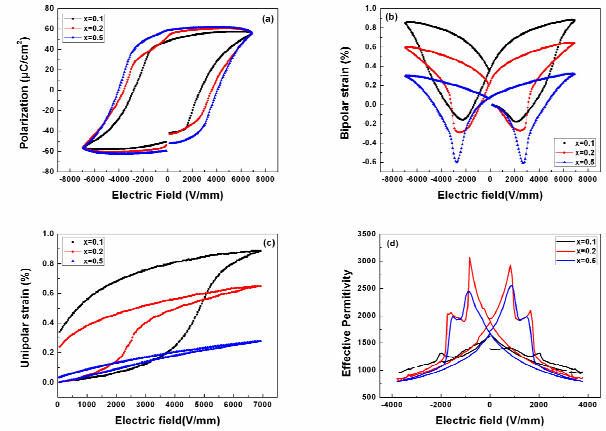


**Fig. 1**. (a) Polarization hysteresis loops (*P-E*), (b) bipolar strain curves (*S-E*); (c) unipolar strain (*S-E*) curves and (d) electric field dependent effective permittivity ε for x%-Fe:NBBT5 single crystals.

## 3. Results and discussion

### 3.1 Results

Fig. 1(a) shows *P-E* hysteresis loops for x%-Fe:NBBT5 single crystals, in which well-saturated loops were observed. With increasing Fe doping concentration, more and more saturated polarization loops with higher coercive field $E_c$, larger maximum polarization $P_{max}$ and remnant polarization $P_{rem}$ were observed. The values of $P_{rem}$ and $E_c$ for 0.5%-Fe:NBBT5 single crystals are 58.7 μC/cm$^2$ and 4.0 kV/mm, respectively. Fig. 1(b) shows bipolar strain curves (*S-E*) for Fe:NBBT5 single crystals. The relative large remnant strain $S_{rem}$ in 0.1%-Fe:NBBT5 implies the non-ergodic feature of pure NBT-BT ferroelectrics,[5] i.e., the field-induced ferroelectric phase cannot fully transform irreversibly into non-polar phase upon the removal of the external field. With further increasing the Fe doping concentration, the electric-field-induced strain hysteresis loops evolves from 'sprout'- to butterfly-shape. Besides, the remanent strain decreases and the negative strain $S_{neg}$ develops gradually. The negligible remanent strain in 0.5%-Fe:NBBT5 indicates a transition from 'non-ergodic' to 'ergodic' relaxor state, making the crystals more suitable for electromechanical devices. These changes suggest that the stability of field-induced ferroelectric order is enhanced and the transformation of macroscopically nearly 'nonpolar' phase to ferroelectric order at zero electrical field is improved.[14, 15] The maximum field-induced bipolar strains for 0.1%-Fe:NBBT5, 0.2%-Fe:NBBT and 0.5%-Fe:NBBT5 are 1.08, 0.95 and 0.89 %, respectively. The unipolar strain hysteresis (*ε-E*) loops share the same feature of electric-field response with the bipolar strain, as shown in Fig. 1(c). With increasing iron doping concentration, the hysteresis becomes smaller and smaller and nearly linear and anhysteretic *ε-E* curve was observed for 0.5%-Fe:NBBT5 single crystals. The values of normalized strain $\varepsilon_{max}/E_{max}$ for 0.1%-Fe:NBBT5, 0.2%-Fe:NBBT5 and 0.5%-Fe:NBBT5 single crystals are 1285.7, 928.6 and 428.61 pm/V, respectively.

The effective permittivity ε response to electric bias field also displays the ferroelectric switching feature, as shown in Fig. 1(d). Only slightly change in ε was observed in 0.1%-Fe:NBBT5 upon application of electric bias field, where ε at maximum field is 959 compared with a zero field value of 1500. However, more obvious response behavior of permittivity to dc bias was observed in 0.2%-Fe:NBBT5 single crystals: with increasing electric field, the permittivity increases dramatically and a sharp peak valued by 3071 at 1 kV/mm was observed. This is followed by a fast decrease and then a slightly increase and a shoulder at around 1.2 kV/mm. At high field, the hysteresis becomes smaller and the permittivity decreases gradually. The permittivity of 0.5%-Fe:NBBT5 single crystals evolves similarly to that of 0.2%-Fe:NBBT5. The increasing iron doping concentration reduces the permittivity at maximum dc field (e.g., 3 kV/mm) from 959 to 794 and then to 792. The relative deviation can be calculated according to Eq. 1:[16]

$$\Delta\varepsilon = \frac{\varepsilon_{max} - \varepsilon_{min}}{\varepsilon_0} \qquad (1)$$

where $\varepsilon_{max}$ is the maximum permittivity, $\varepsilon_{min}$ is the minimum permittivity, and $\varepsilon_{0kV}$ is the permittivity at zero field. The measured permittivity was found to be tuneable by up to 120% and 98% under the application of electrical field for 0.2%-Fe:NBBT5 and 0.5%-Fe:NBBT5, respectively.

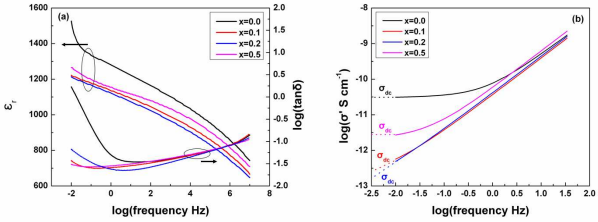


**Fig. 2**. (a) frequency dependent dielectric constant $\varepsilon_r$ and loss factor tanδ and (b) frequency dispersion of the conductivity, which approaches the dc conductivity $\sigma_{dc}$ at low frequencies.

Fig. 2(a) shows the dielectric constant $\varepsilon_r$ and dielectric loss tanδ as a function of frequency measured at room temperature. With increasing frequency, the dielectric properties show a relaxation behavior as the dielectric constant $\varepsilon_r$ decreases gradually in the whole frequency range while the loss factor tanδ

decreases quickly in the low frequency range ($10^{-2}$<f<10 Hz) but increases in the high frequency range (f>10 Hz). It is clear that iron doping decreases both of the $\varepsilon_r$ and tanδ effectively, especially at the low frequency range (f<10 Hz). Fig. 2(b) illustrates the potential of the room temperature dc conductivity $\sigma_{dc}$ suppression in x%-Fe:NBBT5 single crystals. The $\sigma_{dc}$ can be estimated by extrapolating the so-called "dc-plateau"of the $\sigma'(\omega)$, which is mainly contributed by long-range charge migration.[17, 18] It can be seen that $\sigma_{dc}$ is reduced at least one order of magnitude after iron doping. However, an abnormal increase in $\sigma_{dc}$ was observed in 0.5%-Fe:NBBT5 single crystals as compared with 0.1- and 0.2%-Fe:NBBT5 single crystals.

The representative parameters of electrical property for NBT-BT single crystals were compared with PZT ceramics and were summarized in Table I. Compared to pure NBBT5, the dielectric constant $\varepsilon_r$ and dielectric loss tanδ are reduced, while the piezoelsetric constant $d_{33}$ is improved obviously. The highest $d_{33}$ was found in 0.2%-Fe:NBBT5 single crystals, which is 590 pC/N. Besides, a dramatic enhancement in the remnant polarization $P_r$ (~500%) and coercive field $E_c$ (~200%) after iron doping were observed. Furthermore, the ultrahigh field-induced bipolar and unipolar strains make it possible to substitute PZT ceramics in electromechanical device applications.

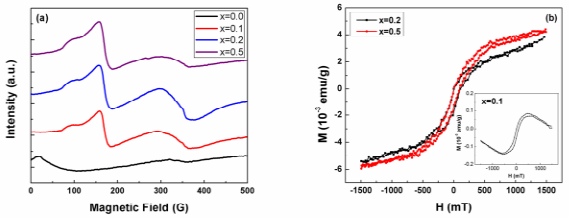


**Fig. 3**. (a) X-band (9.8 GHz) EPR spectra and (b) the *M-H* curves for x%-Fe:NBBT5 single crystals measured at room temperature.

The electronic configuration of free trivalent iron ions is $3d^5$. Thus, the ground state of $Fe^{3+}$ is $^6S_{5/2}$ with S=5/2. The $Fe^{3+}$-degeneracy in a crystal field is lifted to three Kramer's doublets due to international electric field gradients. The remaining degeneracy may be lifted by an external magnetic field resulting in six Zeeman levels. Therefore, the two resonances at low field (100 and 180 mT) are characteristic features that demonstrate the formation of $(Fe'_{Ti}-V_O^{\bullet\bullet})^{\bullet}$ defect complexes in the crystal lattice.[10, 12] Namely, the valence of Fe was +3 and $Fe^{3+}$ substitutes $Ti^{4+}$ ions at B-site. The silent EPR spectrum for x=0.0 at 100 and 180 mT indicates that no defect centers arose from iron ions exist in pure NBBT5 single crystals. The broad peaks located at around 340 mT can be assigned to the formation of magnetoplumbite second phase in the crystal lattice.[20] This is confirmed by the room-temperature *M-H* hysteresis curves for x%-Fe:NBBT5 single crystals, as shown in Fig. 3(b). Similar to $PbTiO_3$,[23] the diamagnetic contributions from the host NBT-BT results in the decrease of the magnetization at larger magnetic field strength part in 0.1%-Fe:NBBT5 single crystals (the inset in Fig. 3(b)). However, further increase the iron doping concentration transits the *M-H* curve gradually into the typical S-type hysteresis curves. The $M_s$ for 0.2%- and 0.5%-Fe:NBBT5 single crystals is ~$4.0\times10^{-3}$ emu/g, indicating the emerging of ferromagnetic long-rang ordering.

For NBT-based ferroelectrics, the high volatility of bismuth at high temperature during sample synthesis is usually compensated by oxygen vacancies, which are always considered as mobile and gives rise to the n-type conductivity in this class of materials.[24-26] Fig. 4(a) shows temperature dependent complex impedance spectra of 0.1%-Fe:NBBT5 single crystals from 40 to $10^6$ Hz. The single semicircles indicate the conduction is dominated by one relaxation mechanism in a wide temperature range. Similar behavior was also observed in 0.2%-Fe:NBBT5 and 0.5%-Fe:NBBT5 single crystals, as depicted in Fig. 4(b) and (c), respectively. The values of resistivity (R) were derived by extrapolating the low-frequency intercept of the simulated semicircles with real axis. The high temperature conductivity $\sigma$ can be calculated using $\sigma = l/RS$, where l and S are the thickness and cross-section area of the samples', respectively. Then the activate energy ($E_a$) can be fitted using the Arrhenius equation:

$$\sigma = \sigma_0 \exp(-E_a/kT) \qquad (2)$$

where $\sigma_0$ is a constant, k is the Boltzmann constant and T is the absolute temperature. The logarithms of σ vs. 1000/T were plotted in Fig. 4(d). The solid lines are the best least-squares fitting of Eq. (2). The activation energies for pure NBBT5, 0.1%-Fe:NBBT5, 0.2%-Fe:NBBT5 and 0.5%-Fe:NBBT5 were obtained, which are 0.624, 0.507, 0.524 and 0.545 eV, respectively, indicating the electromigration of oxygen vacancies dominates the conductivity.[24, 27] The decrease in $E_a$ after iron doping is attributed the increased concentration of oxygen vacancies. The effects of iron doping on conductivity were demonstrated to phenomenologically follow the same behavior as room temperature dc conductivity: the $Fe'_{Ti}$ functional centers interact with oxygen vacancies and therefore hinder their migration, resulting in the depressed conductivity in 0.1%-Fe:NBBT5 and 0.2%-Fe:NBBT5. Nevertheless, the increased conductivity in 0.5%-Fe:NBBT5 single crystals suggests that the depression of charge carriers' mobility is overwhelmed by the largely increased concentration of the extrinsic oxygen vacancies.

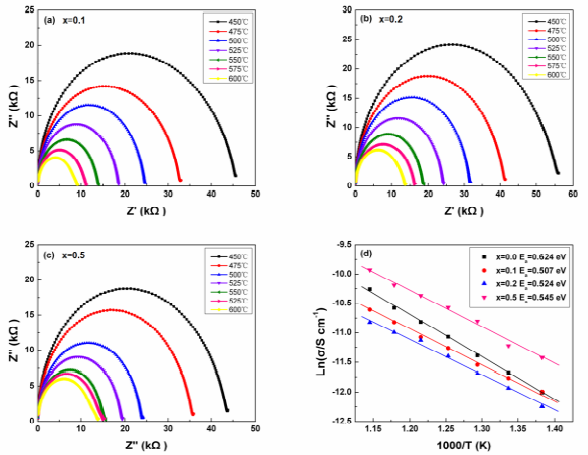


**Fig. 4**. Temperature dependent complex impedance spectra measured from 40 to $10^6$ Hz: (a) 0.1%-Fe:NBBT5; (b) 0.2%-Fe:NBBT5; (c) 0.5%-Fe:NBBT5 and (d) Arrhenius plot of conductivity for x%-Fe:NBBT5 single crystals.

Similar to Mn doped single crystals and CuO doped ceramics, the partially charge-compensated $(Fe'_{Ti}-V_O^{\bullet\bullet})^{\bullet}$ defect dipoles introduce a tetragonal crystalline field and strong tetragonal ferroelectric distortion,[27-29] which inhibit the development of the long-range ferroelectric order and act as nucleation centers of tetragonal orders. Therefore, the formation of fine-domain structures is improved and domain size is notably reduced from broad bands in pure NBBT5 single crystals into fine platelets in iron doped NBBT5 single crystals, as depicted in Fig. 5(a)-(d). The optical extinctions for pure NBBT5 and 0.1%-Fe:NBBT5 single crystals were found at θ=45°+m · 90° (m=0, 1, 2 and 3), which is the typical extinction position for

rhombohedral structures.[30, 31] Further increasing the iron doping concentration, the domain platelets become more and more finer and regions with complete extinction for θ = 0° + m · 90° (m = 0, 1, 2 and 3) develop gradually, indicating domains with rhombohedral symmetry evolve into tetragonal structures in 0.2%-Fe:NBBT5 and 0.5%-Fe:NBBT5 single crystals.

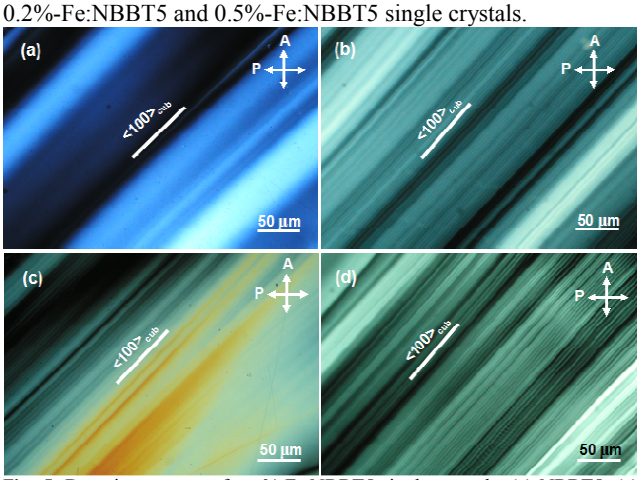


**Fig. 5**. Domain structures for x%-Fe:NBBT5 single crystals: (a) NBBT5; (a) 0.1%-Fe:NBBT5; (c) 0.2%-Fe:NBBT5 and (d) 0.5%-Fe:NBBT5.

The ultrahigh piezoelectric response in x%-Fe:NBBT5 single crystals can be rationalized by the incorporation of $(Fe'_{Ti} - V_O^{\bullet\bullet})^{\bullet}$ defect dipoles and their interactions with charge carriers and domain structures. The reduced leakage current density necessarily increases the effective field when applying an external electric field on x%-Fe:NBBT5 single crystals. Besides, the strong tetragonal ferroelectric distortion improves the intrinsic contributions, i.e., the lattice distortion, deformation of single domains. At the same time, the increased domain wall density enhances the extrinsic contributions, which mainly result from the movement of domain walls responding to the cycling of electric field.[32-34] Therefore, the effective permittivity responding to electric bias field is more and more pronounced (Fig. 1). What's more, although the pinning of defect dipoles on domain walls results in the increased coercive field, the enhanced stabilization of tetragonal symmetry benefits the field-induced phase transformation from rhombohedral to tetragonal phase. Therefore, the stability of field-induced ferroelectric order is improved, resulting in the enhanced $P_r$ and $S_{neg}$ in x%-Fe:NBBT5 single crystals. However, the increased volume fraction of tetragonal phase decreases the field-induced strains contributed by this field-induced phase transformation process, resulting in the more and more depressed hysteresis in the unipolar strain curves. The decreased permittivity tunability in 0.5%-Fe:NBBT5 with regard to 0.2%-Fe:NBBT5 is attributed to the increased leakage current density and dielectric loss.

## Conclusions

In summary, the effects of microscopic defect structure on macroscopic properties have been in x%-Fe:NBBT5 (x=0.1, 0.2 and 0.5) single crystals have been studied systematically. EPR spectra reveal that the valence of Fe was +3 and $Fe^{3+}$ substitutes $Ti^{4+}$ ions at B-site. The $Fe'_{Ti}$ functional centers interact with oxygen vacancies and therefore hinder their electromigration. Besides, the formation of $(Fe'_{Ti} - V_O^{\bullet\bullet})^{\bullet}$ defect dipoles reduces domain size and improves the evolution from rhombohedral to tetragonal phases. These transformations in the local structure depress the leakage current density and dielectric loss effectively, leading to the ultrahigh ferroelectric response in x%-Fe:NBBT5 single crystals. The presence of ferromagnetic properties in x%-Fe:NBBT5 single crystals further provides new application potential as multiferroic materials.

## Acknowledgements

This work was financially supported by the Ministry of Science and Technology of China through 973 Program (No. 2013CB632902), the Natural Science Foundation of China (Nos. 51332009, 51372258, 11304333 and 51272268)

## Notes and References

[a] *Key Laboratory of Inorganic Functional Materials and Devices, Shanghai Institute of Ceramics, Chinese Academy of Sciences 215 Chengbei Road, Jiading, Shanghai, 201800, China*
[b] *Graduate University of Chinese Academy of Sciences, Beijing, 100049, China*
*Fax: +8621-5992-7184; Tel: +8621-6998-7759;*
*E-mail: zhw3789@sina.com and hs1uo@mail.sic.ac.cn*

1 V. Dorcet, G. Trolliard, and P. Boullay, *Chem. Mater*. 2008, 20, 5061.
2 M. Spreitzer, M. Valant, and D. Suvorv, *J. Mater. Chem*, 2007, **17**, 185.
3 C. Ma, H. Guo, S. P. Beckman, X. Tan, *Phys. Rev. Lett*. 2012, **109**, 107602.
4 R. Dimmer, E. Aulbach, W. Jo, K. G. Webber, and J. Rödel, *Script. Mater*. 2012, **67**, 100.
5 W. Jo, R. Dittmer, M. Acosta, J. Zang, C. Groh, E. Sapper, K. Wang, J. Rödel, *J. Electroceram*. 2012, **29**, 71.
6 R.-A. Eichel, H. Meštrić, H. Kungl, and M. J. Hoffmann, *Appl. Phys. Lett*. 2006, **88**, 122506.
7 R.-A. Eichel, P. Erhart, P. Träskenlin, K. Albe, H. Kungl, and M. J. Hoffman, *Phys. Rev. Lett*. 2008, **100**, 095504.
8 R.-A. Eichel, *J. Am. Ceram. Soc*. 2008, **91,** 691.
9 M. I. Morozov, and D. Damjanovic, *J. Appl. Phys*. 2010, **107**, 034106.
10 P. Erhart, R.-A. Eichel, P. Träskelin, and K. Albe, *Phys. Rev. B* 2007, **71**, 174116.
11 V. S. Postinkov, V. S. Pavlov, S. K. Turkov, *J. Phys. Chem. Solids*.1970, **31**, 1785.
12 P. Jakes, E. Erdem, R-A. Eichel, L. Ji, and D. Damjanovic, *Appl. Phys. Lett*. 2011, **98**, 072907.
13 Q. Zhang, X. Zhao, R. Sun, and H. Luo, Phys. *Status. Solidi A*. 2011, **208**, 1012.
14 W. Jo, T. Granzow, E. Aulbach, J. Rödel, D. Damjanovic, *J. Appl. Phys*. 2009, **105**, 094102 .
15 W. Jo, E. Erdem, R-A. Eichel, J. Glaum, T. Granzow, D. Damjanovic, J. Rödel, J. Appl. Phys. 2010, **108**, 014110.
16 R. Dimmer, W. Jo, J. Daniels, S. Schaab, J. Rödel, *J. Am. Ceram. Soc*. 2011, **94**, 4283.
17 M. I. Morzov, and D. Damjnaovic, J. Appl. Phys. 2010, **107**, 034106.
18 M. I. Morzov, M.-A. Einarsrud, and T. Grande, *Appl. Phys. Lett*. 2014, **104**, 122905.
19 S. E. Park, T. R. Shrout, *J. Appl. Phys*. 1997, **82**, 1804.
20 T. R. Shrout, and S. J. Zhang, *J. Electroceram*. 2007, **19**, 111.
21 S-T. Zhang, A. B. Kounga, E. Aulbach, T. Granzow, W. Jo, H-J. Kleebe, J. Rödel, *J. Appl. Phys*. 2008, **103**, 034107.
22 H-J. Kleebe, S. Lauterbach, L. Silvestroni, H. Kungl, M. J. Hoffmann, E. Erdem, R-A. Eichel, *Appl. Phys. Lett*. 2009, **94**, 142901.
23 Z. Ren, G. Xu, X. Wei, Y. Liu, X. Hou, P. Du, W. Weng, G. Shen, and G. Han, *Appl. Phys. Lett*. 2007, **91**, 063106.
24 M. Li, M. J. Pietrowski, Roger A. De Souza, H. Zhang, I. M. Reaney, S. N. Cook, J. A. Kilner, D. C. Sinclair, *Nature. Mater*. 2014, **13**, 31.
25 Y. Hiruma, H. Nagata, and T. Takennaka, *J. Appl. Phys*. 2009, **105**, 084112.
26 H. Zhang, C. Chen, X. Zhao, H. Deng, L. Li, D. Lin, X. Li, B. Ren, H. Luo, and J. Yan, *Appl. Phys. Lett*. 2013, **103**, 212906.




This journal is © The Royal Society of Chemistry [2014]

27 H. Zhang, H. Deng, C. Chen, L. Li, D. Lin, X. Li, X. Zhao, H. Luo, and J. Yan, *Scrip Mater*. 2014, **75**, 50.
28 J. Yao, Y. Yang, N. Monsegue, Y. Li, J. Li, Q. Zhang, Q. Zhang, H. Luo, and D. Viehland, *Appl. Phys. Lett*. 2011, **98**, 1432903.
29 M. Ehmke, J. Glaum, W. Jo, T. Granzow, and J. Rödel, *J. Am. Ceram. Soc*.2011, **94**, 2473.
30 Z.-G. Ye, M. Dong, *J. Appl. Phys*. 2000, **87**, 2312.
31 J. Yao, L. Yan, W. Ge, L. Luo, J. Li, D. Viehland, Q. Zhang and H. Luo, *Phys. Rev. B*. 2011, **83**, 054107.
32 D. Damjanovic, *J. Am. Ceram. Soc*. 2005, 88, 2663.
33 F. Li, S. Zhang, Z. Xu, X. Wei, J. Luo, and T. R. Shrout. *J. Appl. Phys*. 2010, **108**, 034106.
34 Z-Y. Shen, Y. Tang, S. Zhang, J. Luo, Y. Li, and T. R. Shrout, *Scrip Mater*. 2014, 72-73, 17.

**TABLE I**. Electrical properties of NBT-BT single crystals as compared to PZT and other NBT-based ceramics.

| | $\varepsilon_r$ | tanδ (%) | $P_r$ (μC/cm$^2$) | $E_c$ (kV/mm) | $d_{33}$ (pC/N) | $S_{max}$ (%) | $\varepsilon_{max}/E_{max}$ (pm/V) | Ref. |
|---|---|---|---|---|---|---|---|---|
| Hard PZT, PZT8 | 1000 | 0.4 | ~20 | ~2.2 | 225 | - | 150 | 19, 20 |
| Soft PZT, PZT-5H | 3400 | 2.0 | ~32 | 0.6-0.8 | 590 | - | 400-590 | 19, 20 |
| NBT-6BT-2KNN | 2320 | 6.2 | 16 | 1.3 | 30 | 0.45 | 567 | 21 |
| Pure NBBT5 | 1100 | 2.7 | 11.8 | 2.2 | 420 | 0.12 | 249.6 | This work |
| 0.1%-Fe:NBBT5 | 988 | 1.5 | 48.3 | 2.7 | 478 | 1.08 | 1285.7 | This work |
| 0.2%-Fe:NBBT5 | 964 | 2.1 | 53.2 | 3.5 | 590 | 0.95 | 928.6 | This work |
| 0.5%-Fe:NBBT5 | 1034 | 1.9 | 58.7 | 4.0 | 525 | 0.89 | 428.6 | This work |